NAG1-886

NASA Contractor Report

A FIRST SCRAMJET STUDY

George Emanuel
School of Aerospace and Mechanical Engineering
The University of Oklahoma
Norman, Oklahoma

NASA Contractor Report

A FIRST SCRAMJET STUDY

George Emanuel
School of Aerospace and Mechanical Engineering
The University of Oklahoma
Norman, Oklahoma

CONTENTS

SUMMARY

This report documents a variety of related scramjet engine topics in which primary emphasis is on simplicity and conceptual clarity. Thus, the flow is assumed to be one dimensional, the gas is thermally and calorically perfect, and the study focuses on low hypersonic Mach numbers. The first technical section evaluates the thrust and lift of an exposed half nozzle, which is used on the aero-space plane, as well as one that is fully confined. A rough estimate is provided of the drag of an aero-space plane. Background material dealing with thermal effects and shock waves is discussed in the next section. The following section then presents a parametric scramjet model, based on the influence coefficient method, that evaluates the dominant scramjet processes. The independent parameters are the ratio of specific heats, a nondimensional heat addition parameter, and four Mach numbers. The total thrust generated by the combustor and nozzle is shown to be independent of the heat release distribution and the combustor exit Mach number, providing thermal choking is avoided. An operating condition for the combustor is found that maximizes the thrust. An alternative condition is explored when this optimum is no longer realistic. This condition provides a favorable pressure gradient and a reasonable area ratio for the combustor. The next section provides parametric results based on the model. One significant finding is the sensitivity of the thrust to the value of the ratio of specific heats for the air upstream of the combustor. The final section summarizes and discusses the analysis.

INTRODUCTION

In recent years, there has been a renewed interest in scramjet engines. These engines operate at hypersonic vehicle speeds, and the flow internal to the engine is supersonic. Above a free-stream Mach number of about 5, a

ramjet engine is no longer viable. Only a scramjet or rocket engine can provide a significant thrust in this flight regime. For powered flight in the atmosphere over a long distance, only a scramjet engine is suitable, since the ambient air replaces the rocket's stored oxidizer.

Conceptually, a scramjet engine is simple, although the problems associated with it are severe and some of them are still unresolved. For instance, one of these problems is the difficulty of performing appropriate tests at hypersonic flight Mach numbers. Because of this difficulty, there has been an effort to computationally model the engine and its inlet (see references 1 and 2). Over the past 30 years, there have also been a number of system-oriented models (see references 3-7). However, it is often difficult to assess the validity of these models. They frequently utilize correlation formulas and numerous efficiency or fudge factors. Despite these factors, it is not evident that the analysis adheres to the governing conservation laws of fluid dynamics.

In this report, a variety of issues are discussed. In each instance, emphasis is on simplicity and conceptual clarity. A primary objective of this effort is tutorial where we place the scramjet engine within a simple theoretical framework. Nevertheless, we are not aware of a similar document in the journal literature or among those reports in our possession. Consequently, certain aspects of the analysis may be new.

To lay the groundwork for the subsequent discussion, we evaluate the thrust and lift of an exposed half nozzle and one that is fully confined. The next section then concludes with a rough estimate of the drag of an aero-space plane. This estimate is needed to calibrate subsequent thrust estimates. The following section presents background material, which is useful in the subsequent sections. Thermal considerations and shock waves are the principal

topics discussed. A parametric scramjet model, based on the influence coefficient method, is then provided. Although elementary, the model evaluates some of the dominant scramjet processes to first order. Results based on the model are presented in an extensive series of tables, while the final section summarizes our findings.

SYMBOLS

a	speed of sound
A	cross-sectional area
B,C	fixed parameters in equation (47)
C_D	drag coefficient
C_f	skin-friction coefficient
D	drag
D	hydraulic diameter
$\hat{e}_x, \hat{e}_y$	unit vectors along the x and y axis
F	impulse function
I_{sp}	specific impulse
L	lift
$\dot{m}$	mass flow rate per unit depth
$\dot{m}_f$	fuel mass flow rate
M	Mach number
$\hat{n}$	unit normal vector
p	pressure
q	heat addition per unit mass
Q	nondimensional heat addition
Q_R	maximum heat addition in Rayleigh flow
R	gas constant
S	surface area

S_p planform area

T temperature

V flow speed

$\vec{V}$ velocity

x,y Cartesian coordinates

$\mathcal{T}$ thrust

α defined by equation (53)

γ ratio of specific heats

μ Mach angle

ρ density

ϕ equivalence ratio

subscripts and superscripts

B end of kernel region on lower wall (see figure 3)

c confined nozzle

d downstream of a normal shock wave

e exposed half nozzle

f nozzle exit

i inlet

is isentropic

j lower edge of jet

mx maximum

u upstream of a normal shock wave

w wall

wℓ lower wall

wu upper wall

0 stagnation

1 combustor inlet

1-2	combustor
1-3	combustor plus nozzle
2	combustor exit or nozzle inlet
3	nozzle exit
∞	free stream
$( )^*$	M = 1 condition
$\hat{( )}$	dimensional value

FORCE DISCUSSION

Figure 1 shows a conventional sketch of an aero-space plane in hypersonic flight. The afterbody consists of what we call an exposed half nozzle. Internal to the scramjet engine, a high pressure and temperature gaseous state is achieved. This state is a result of some compression by the forebody itself and its bow shock wave, by the scramjet's inlet, and by air/fuel combustion downstream of the inlet. Generally, some expansion occurs inside the engine before the inlet to the exposed half nozzle is reached, where a further expansion occurs. Both expansions, internal and external, generate thrust. Later, we evaluate the total thrust. These later sections show that internally generated thrust is quite important.

Our discussion in this section is confined to the exposed half nozzle, which produces both lift and thrust. Lift production, on the other hand, does not occur in the internal nozzle, where the flow field is approximately symmetric. If the vehicle were a rocket, the thrust nozzle would be fully enclosed. An exposed half nozzle is used to reduce the vehicle's weight, size, and heat transfer load. We anticipate that the lift may be of secondary importance relative to the lift generated by the forebody.

Our objective in this section is to derive simple formulas for the lift and thrust developed by the exposed nozzle. For the subsequent analysis, we

need similar relations for an enclosed bell-shaped thrust nozzle. Our starting point utilizes the integral relations developed in references 8 and 9 for waverider vehicles. This approach is most conveniently found in section 20.3 of reference 10. (In the subsequent discussion, we shall often have recourse to this reference.)

The equations for mass and momentum of a steady, inviscid flow can be written as

$$\int_S \rho \, \vec{V} \cdot \hat{n} ds = 0 \tag{1}$$

$$\int_S [\rho \vec{V} (\vec{V} \cdot \hat{n}) + p\hat{n}] ds = 0 \tag{2}$$

where ρ, $\vec{V}$, and p are the density, velocity, and pressure, respectively. The integrals are over a simple closed surface S, which has an outward unit normal vector $\hat{n}$. Aside from the previously mentioned assumptions, we also assume a two-dimensional flow of unit depth.

Confined Nozzle

Figure 2 shows a typical divergent nozzle with uniform inlet and outlet flows. The inlet and exit Mach numbers, M_i and M_f, are arbitrary, although for the subsequent comparison with an exposed nozzle we assume

$$1 \leqslant M_i < M_f \tag{3}$$

The inlet and exit areas are y_i and y_f, as shown in the figure. The enclosing surface consists of three sections, i.e., S_i, S_f, and S_w, where the upper and lower wall surfaces are symmetrical. On these surfaces, we have:

$$\vec{V}_i = V_i \hat{e}_x, \quad \hat{n} = -\hat{e}_x \qquad \text{on } S_i \tag{4a}$$

$$\vec{V}_f = V_f \hat{e}_x, \quad \hat{n} = \hat{e}_x \qquad \text{on } S_f \tag{4b}$$

$$\vec{V} \cdot \hat{n} = 0 \qquad \text{on } S_w \tag{4c}$$

With these relations, equations (1) and (2) become

$$\dot{m} = (\rho V y)_i = (\rho V y)_f \tag{5}$$

$$-\left(\rho V^2 y\right)_i \hat{e}_x - (py)_i \hat{e}_x + \int_{S_w} p\hat{n} ds + \left(\rho V^2 y\right)_f \hat{e}_x + (py)_f \hat{e}_x = 0 \tag{6}$$

where $\dot{m}$ is the mass flow rate per unit depth, and $\hat{e}_x$ and $\hat{e}_y$ are unit Cartesian vectors along their respective coordinates.

As indicated in figure 2, we assume the upstream velocity $\vec{V}_i$ and nozzle exit velocity $\vec{V}_f$ are parallel. The lift L and thrust $\mathcal{T}$, relative to $\vec{V}_i$, are then defined by

$$L = \hat{e}_y \cdot \int_{S_w} p\hat{n} ds \tag{7}$$

$$\mathcal{T} = -\hat{e}_x \cdot \int_{S_w} p\hat{n} ds \tag{8}$$

respectively. With the use of equations (5) and (6), we readily obtain

$$L_c = 0 \tag{9}$$

$$\mathcal{T}_c = (py + \dot{m}V)_f - (py + \dot{m}V)_i = F_f - F_i \tag{10}$$

where a c subscript denotes a confined nozzle, and the impulse function F is defined as

$$F = pA + \rho V^2 A \tag{11}$$

As expected, the thrust $\mathcal{T}_c$ is simply the difference between the inlet and exit values of the impulse function.

It is worth noting that equation (10) is not directly applicable to a conventional thrust rocket (see reference 11). Our analysis, therefore, is not appropriate for this propulsion device.

Exposed Half Nozzle

Figure 3 shows a schematic of an exposed nozzle. The inlet and exit flows are again uniform and parallel with the same inlet and exit areas as for the confined nozzle. The flow is confined by an upper wall S_{wu} and a lower wall $S_{w\ell}$ that extends from the origin to point B on the x-axis. The shape of the upper wall can be based on the theory for a two-dimensional minimum length nozzle with a planar inlet surface (see reference 10), although this specific configuration is not necessary for our purposes. In any case, the flow field should be viewed as the upper half of that for a confined symmetric nozzle. The flow is uniform downstream of the BC Mach line, which is straight. It is simpler, however, to use for the enclosing surface the sum of five surfaces

$$S = S_i + S_{wu} + S_f + S_j + S_{w\ell}$$

where S_j is along the exposed lower edge of the jet and S_f is perpendicular to $\vec{V}_f$. For this analysis, inequalities (3) are required.

On S_i, S_f, and S_{wu}, equations (4) still hold. On the remaining two surfaces, we have

$$\vec{V}\cdot\hat{n} = 0, \quad \hat{n} = -\hat{e}_y \qquad \text{on } S_{w\ell} \text{ and } S_j \tag{12}$$

Equations (1) and (2) now yield equations (5) and

$$-F_i\hat{e}_x + \int_{S_{wu}} p\hat{n}ds + F_f\hat{e}_x - \left[\int_0^{x_B} p dx + p_f(x_f - x_B)\right]\hat{e}_y = 0 \tag{13}$$

The exposed nozzle, denoted by an e subscript, provides a lift L_e given by

$$L_e = \hat{e}_y \cdot \left[\int_{S_{wu}} p\hat{n}ds\right] - \int_0^{x_B} p dx$$

where the rightmost integral is along $S_{w\ell}$. By multiplying equation (13) with $\cdot\hat{e}_y$, we obtain

$$L_e = p_f(x_f - x_B) \tag{14}$$

Hence, the nozzle has a positive lift. Its magnitude is quite small, compared to the forebody's lift, because p_f is generally small. Additionally, the nozzle contributes a pitching moment about the nose of the vehicle, which should not be neglected.

In view of the parallel flow in both the inlet and exit planes, it may seem strange that the nozzle has a non-zero lift. However, the same result is obtained by summing the $\hat{e}_y$ components of the forces on the fluid inside the closed surface S. By Newton's second law, these sum to zero. Basically, our L_e result stems from the asymmetry of an exposed half nozzle.

Equation (14) can be put into a more convenient form by observing that the BC Mach line is at a Mach angle μ_f, where

$$\frac{y_f}{x_f - x_B} = \tan\mu_f = \left(M_f^2 - 1\right)^{-1/2} \tag{15}$$

The area ratio, y_f/y^*, where by definition $M^* = 1$, is provided by the isentropic relation

$$\frac{y_f}{y^*} = \left(\frac{2}{\gamma + 1}\right)^{(\gamma+1)/[2(\gamma-1)]} \frac{1}{M_f} \left(1 + \frac{\gamma - 1}{2} M_f^2\right)^{(\gamma+1)/[2(\gamma-1)]} \tag{16}$$

We have now assumed a perfect gas and a constant value for the ratio of specific heats, γ. The pressure p_f is similarly given by

$$p_f = p_0 \left(1 + \frac{\gamma-1}{2} M_f^2\right)^{-\gamma(\gamma-1)} \tag{17}$$

where a zero subscript denotes a stagnation quantity. With the aid of equations (15)-(17), our final expression for the lift is

$$\frac{L_e}{p_0 y^*} = \left(\frac{2}{\gamma + 1}\right)^{(\gamma+1)/[2(\gamma-1)]} \frac{\left(M_f^2 - 1\right)^{1/2}}{M_f \left(1 + \frac{\gamma-1}{2} M_f^2\right)^{1/2}} \tag{18}$$

The thrust of the exposed nozzle $\mathcal{T}_e$ is given by

$$\mathcal{T}_e = -\hat{e}_x \cdot \int_{S_{wu}} p\hat{n} ds$$

This time, we multiply equation (13) by $\cdot\hat{e}_x$, to obtain

$$\mathcal{T}_e = F_f - F_i = \mathcal{T}_c \tag{19}$$

Hence, we have the result that the confined and exposed nozzles have the same thrust. This conclusion is useful in the subsequent modeling where, for simplicity, a confined nozzle is used instead of the actual exposed nozzle shown in figure 1.

Drag Estimate

We need a rough estimate of the drag of an aero-space plane in order to know if our subsequent thrust estimates are sufficient to overcome the drag and provide acceleration. As usual, the drag coefficient is defined as

$$C_D = \frac{2\hat{D}}{(\rho V^2)_\infty S_p} = \frac{2\hat{D}}{\gamma p_\infty M_\infty^2 S_p}$$

where $\hat{D}$ is the dimensional drag, p_∞ and M_∞ are the free stream pressure and Mach number, and S_p is the projected planform area.

For the later scramjet analysis, it is more convenient to introduce a different nondimensional drag given by

$$D = \frac{\hat{D}}{p_\infty A_1} \tag{20}$$

where A_1 is the projected combustor inlet area on a plane perpendicular to $\vec{V}_\infty$. The actual combustor inlet area would be larger if it is canted relative to $\vec{V}_\infty$. We now have

$$D = \frac{\gamma}{2} M_\infty^2 \frac{S_p}{A_1} C_D$$

For our estimate, we utilize

$$\gamma = 1.4 \quad , \quad M_\infty = 7 \quad , \quad \frac{A_1}{S_p} = 10^{-2} \quad , \quad C_D = 6 \times 10^{-2} \tag{21}$$

to obtain

$$D = 206 \tag{22}$$

The C_D estimate in equations (21) is significantly higher than would be

estimated for the forebody drag, even if a turbulent boundary layer is assumed. However, our C_D estimate also includes internal engine viscous drag and, more importantly, the drag associated with compressing the engine air flow from its upstream condition to that at the inlet of the combustor. While the above D value is a crude estimate, it nevertheless is in the range of drag values that can be extracted from reference 7. Due to the $p_\infty A_1$ normalization, D should not rapidly vary with flight altitude. It will vary with M_∞, since the drag due to engine air compression depends on M_∞. This compression, however, also strongly depends on the Mach number at the inlet of the combustor. As a consequence, D is not proportional to M_∞^2.

BACKGROUND DISCUSSION

Overview

We first outline the major assumptions and provide a brief overview of the flow field. The flow is assumed to pass through one, or more, weak oblique shock waves before it reaches the inlet of the combustor. Some of this compression may be isentropic; the amount depends on the vehicle's forebody and engine inlet design. For purposes of simplicity, we assume M_∞ and p_∞ isentropically change to M_1 and p_1 at the inlet of the combustor. Of course, this assumption is optimistic; it should be altered when there is a known configuration upstream of the combustor. Although optimistic, the assumption is not grossly in error as long as the shock waves are weak.

A schematic of the engine is shown in figure 4. It consists of just two units, a combustor and a confined, isentropic nozzle. The flow at each of the four stations is assumed to be uniform as required by our quasi-one-dimensional approach. As the figure indicates, the cross-sectional area derivative, dA/dx, is typically discontinuous at the inlet and exit of the combustor. In addition, the flow at station 1 is considered to be sonic or

supersonic. The gas is air, taken as thermally and calorically perfect, with a constant value for the ratio of specific heats γ.

The combustor, located between stations 1 and 2, has a variable cross-sectional area with inviscid flow and with heat addition, which stems from an air-fuel combustion process. We ignore the small additional fuel mass flow rate, the fuel-air mixing process, and any changes in average specific heats or molecular weight. Due to the heat addition, we anticipate that the cross-sectional area ratio A_2/A_1 will exceed unity. Thermal choking is avoided by requiring that $M_2 \geq 1$, where M_2 is to be prescribed.

Between stations 2 and 3, the flow isentropically expands in a nozzle from M_2 to M_3. Later, we use the pressure ratio

$$\frac{p_3}{p_\infty} = \frac{p_3}{p_2}\frac{p_2}{p_1}\frac{p_1}{p_\infty} = \left(\frac{1 + \frac{\gamma-1}{2} M_2^2}{1 + \frac{\gamma-1}{2} M_3^2}\right)^{\gamma/(\gamma-1)} \left(\frac{1 + \frac{\gamma-1}{2} M_\infty^2}{1 + \frac{\gamma-1}{2} M_1^2}\right)^{\gamma/(\gamma-1)} \frac{p_2}{p_1} \tag{23}$$

where p_2/p_1 is evaluated in the analysis section and

$$\frac{p_3}{p_2} = \left(\frac{1 + \frac{\gamma-1}{2} M_2^2}{1 + \frac{\gamma-1}{2} M_3^2}\right)^{\gamma/(\gamma-1)} \tag{24}$$

We also need the nozzle area ratio

$$\frac{A_3}{A_2} = \frac{M_2}{M_3}\left(\frac{1 + \frac{\gamma-1}{2} M_3^2}{1 + \frac{\gamma-1}{2} M_2^2}\right)^{(\gamma+1)/[2(\gamma-1)]} \tag{25}$$

A Brayton cycle, which models a jet engine, consists of an isentropic

compression, followed by constant pressure heat addition, which is then followed by an isentropic expansion. Our engine differs from this cycle in that the heat addition need not occur at a constant pressure. In a conventional Brayton cycle, where the heat addition is subsonic, the constant pressure assumption is realistic. However, for heat addition in a supersonic flow, this assumption is no longer warranted.

Our objective is to determine the thrust $\mathcal{T}_{1-2}$ provided by the combustor and the thrust $\mathcal{T}_{1-3}$ of the overall system. A second objective is to evaluate various pressure, temperature, and area ratios. In view of the parametric nature of the study, care must be taken to avoid unrealistic parameter values. These ratios assist in deciding this issue.

Combustion

We presume a steady combustion process can occur at supersonic speeds. Early scramjet studies were unsure on this point. The issue, however, is now mute in view of the success of the cw supersonic chemical laser. In both devices, fuel and oxidizer streams mix at supersonic speeds. After mixing, a steady combustion process occurs providing the local static temperature is sufficient to overcome the activation energy of the exothermic reactions. In line with our one-dimensional assumption, we henceforth ignore the effects of mixing. While this process is important, it is outside the scope of this study.

Because the H_2 fuel is also used to cool the vehicle, we assume a hydrogen-rich mixture whose stoichiometry is represented by

$$2\phi\ H_2 + O_2 + 3.76\ N_2 \rightarrow 2(\phi-1)H_2 + 2H_2O + 3.76N_2$$

where $\phi \geq 1$. The 3.76 nitrogen coefficient is appropriate for air. For stoichiometric combustion, with $\phi = 1$, a simple estimate for the maximum

change in stagnation temperature T_0 yields

$$\Delta T_0 = T_{02} - T_{01} \cong 2000 \text{ K} \tag{26}$$

The maximum heat addition then is

$$q = \frac{\gamma R}{\gamma - 1} \Delta T_0 \cong 2 \times 10^6 \text{ J/kg} \tag{27}$$

where we use air values for γ(= 1.4) and for the gas constant R(= 287 J/kg-K).

Table I is taken from reference 12 and provides typical atmospheric data at several representative altitudes, h, for hypersonic flight. We shall use a nondimensional heat addition parameter, defined as

$$Q = \frac{q}{RT_\infty} \tag{28}$$

Based on Table 1 and equation (27), Q = 30 is a representative value for the maximum amount of heat addition under stoichiometric conditions. Since T_{01} is given by

$$T_{01} = T_{0\infty} = T_\infty \left(1 + \frac{\gamma-1}{2} M_\infty^2\right) \tag{29}$$

the stagnation temperature ratio across the combustor can be written as

$$\frac{T_{02}}{T_{01}} = 1 + \frac{\gamma-1}{\gamma} \frac{q}{RT_{01}} = 1 + \frac{\gamma-1}{\gamma} \frac{Q}{1 + \frac{\gamma-1}{2} M_\infty^2} \tag{30}$$

With a given M_1, it is useful to determine the value for Q, denoted as Q_R, for which the flow in a constant cross-sectional area duct will thermally choke. This is given by Rayleigh line theory as [see pg. 435 of reference 10 with $M_2 = 1$]

$$Q_R = \frac{q}{RT_0^*}\frac{T_0^*}{T_{01}}\frac{T_{01}}{T_\infty} = \frac{\gamma}{2(\gamma^2-1)}\frac{\left(M_1^2-1\right)^2\left(1+\frac{\gamma-1}{2}M_\infty^2\right)}{M_1^2\left(1+\frac{\gamma-1}{2}M_1^2\right)} \tag{31}$$

where T_0^* is a reference (at M = 1) stagnation temperature, and M_1 may be subsonic or supersonic. Figure 5 shows this relation with $\gamma = 1.4$ for two values of M_∞. Thermal choking is avoided in a constant cross-sectional area duct by having $Q_R \geq Q$. Thus, if $M_\infty = 7$ and $Q = 30$, then M_1 must exceed 5 to avoid thermal choking in a duct with a constant cross-sectional area.

For a large thrust, we are interested in Q values that may appreciably exceed Q_R. Thermal choking is then avoided by A_2/A_1 having a non-unity value such that M_2 has its prescribed sonic or supersonic value.

It is also useful to obtain an estimate of the maximum static temperature, T_{mx}, which typically occurs at the exit of the combustor. This estimate is needed for assessing the approximate validity of the non-reacting and calorically perfect gas assumptions. For these assumptions to be reasonable, T_{mx} should not be too large, otherwise real gas effects become very significant. In turn, this limitation restricts M_∞ to the lower range of hypersonic flight Mach numbers. This temperature is obtained as

$$\frac{T_{mx}}{T_\infty} = \frac{T_{mx}}{T_{02}}\frac{T_{02}}{T_{01}}\frac{T_{01}}{T_{0\infty}}\frac{T_{0\infty}}{T_\infty} = \frac{1+\frac{\gamma-1}{2}M_\infty^2}{1+\frac{\gamma-1}{2}M_2^2}\frac{T_{02}}{T_{01}} \tag{32}$$

where $T_{01} = T_{0\infty}$. With specified values for γ and M_∞, this relation yields an upper bound on Q for a given value of T_{mx}/T_∞.

From references 13 and 14, we see that dissociation of equilibrium air is negligible below a temperature of about 2778 K (5000°R). For air at 30 km

(see Table 1), this means that T_{mx}/T_∞ should satisfy

$$\frac{T_{mx}}{T_\infty} \leqslant \frac{2778}{227} = 12.2$$

Our parametric study will usually adhere to this limit. On the other hand, equilibrium vibrational excitation of the O_2 and N_2 molecules becomes significant at a much lower temperature. For instance, for equilibrium air, γ = 1.294 at 2778 K (see reference 14). While vibrational excitation is not included in the subsequent model, we will make a rough estimate of its effect on the thrust.

Thrust

As equations (10) and (11) show, the thrust is given by the difference in the impulse function at the exit and inlet stations. For the problem at hand, the thrust provided by the combustor is

$$\hat{\mathcal{F}}_{1-2} = F_2 - F_1 = F_1\left(\frac{F_2}{F_1} - 1\right) \tag{33}$$

where a caret denotes a dimensional value. For the overall engine, we have

$$\hat{\mathcal{F}}_{1-3} = F_3 - F_1 = F_1\left(\frac{F_2}{F_1}\,\frac{F_3}{F_2} - 1\right) \tag{34}$$

For a perfect gas, equation (11) can be written as

$$F = pA(1 + \gamma M^2) \tag{35}$$

Since both thrusts are proportional to F_1, it is convenient to define a normalized thrust as

$$\mathcal{Y} = \frac{\hat{\mathcal{Y}}}{P_\infty A_1} \tag{36}$$

This normalization is identical to that used in equation (20) for the drag. It is important to note that equations (33) and (34) hold even when skin friction, a normal shock wave, heat addition, or a gradual change in the cross-sectional area are present.

Impulse Function

With the aid of

$$\dot{m} = \rho A V$$

$$T_0 = T\left(1 + \frac{\gamma - 1}{2} M^2\right)$$

$$a^2 = \frac{\gamma p}{\rho}$$

equation (35) can be written as

$$F = \dot{m}\left(\frac{RT_0}{\gamma}\right)^{1/2} \frac{1 + \gamma M^2}{M\left(1 + \frac{\gamma - 1}{2} M^2\right)^{1/2}} \tag{37a}$$

where a is the speed of sound of a perfect gas. As with equation (35), this relation is a point function; its use in equations (33) and (34) means the intervening flow may contain shock waves, skin friction, an area change, and heat transfer. By evaluating the right side of equation (37a) at M = 1

$$F^* = \left[\frac{2(\gamma + 1)}{\gamma} RT_0\right]^{1/2} \dot{m}$$

we obtain

$$\frac{F}{F^*} = \frac{1 + \gamma M^2}{\left[2(\gamma+1)M^2\left(1 + \frac{\gamma-1}{2} M^2\right)\right]^{1/2}} \tag{37b}$$

where we have assumed T_0 has the same value for F and F^*. Later, this assumption is dropped.

Equation (37b) is shown in figure 6 for $\gamma = 1.4$. For this γ, the asymptotic value of F/F^* is 1.429 as $M \to \infty$. Thus, F/F^* has relatively little variation when the flow is supersonic. Later, equation (37b) is used for the isentropic nozzle flow in the form

$$\frac{F_3}{F_2} = \frac{M_2}{M_3} \frac{1 + \gamma M_3^2}{1 + \gamma M_2^2} \left(\frac{1 + \frac{\gamma-1}{2} M_2^2}{1 + \frac{\gamma-1}{2} M_3^2}\right)^{1/2} \tag{38}$$

The double valued behavior evident in figure 6 can be understood by writing F as

$$F = pA + \dot{m}V$$

where the mass flow rate, $\dot{m}$, is a constant. Consider flow in a duct with a fixed exit area A. At a low subsonic Mach number, V approaches zero while p approaches its stagnation value, thus the pA term dominates. At a high supersonic Mach number, the rightmost term dominates, since p approaches zero whereas V approaches its limiting value. Note that F approaches infinity as $M \to 0$.

The foregoing infinity motivates us to consider an engine with isentropic flow that operates as a shock-free diffuser with a supersonic inlet and a subsonic exit. When M_∞ is large, the engine has a large thrust since a large fraction of the free-stream kinetic energy is converted into internal energy.

The positive thrust stems from a low static pressure on the walls upstream of the throat, where the flow is supersonic, and a large pressure that approaches the stagnation value on the walls downstream of the throat. This thrust does not require any heat addition. By the momentum theorem, it is unaltered if the coordinate system is fixed with the engine, as in our analysis, or the engine is traveling with velocity $\vec{V}_\infty$ into quiescent air.

The foregoing discussion presumes the flow decelerates isentropically to a subsonic value. If the flow remains supersonic everywhere within the converging/diverging duct, it is still possible to obtain a (relatively small) positive thrust, providing the exit area exceeds that of the inlet. In fact, this happens in the subsequent parametric model, i.e., the (inviscid) engine has positive thrust even when the heat addition is zero.

Different definitions for the thrust and drag are common. The definitions typically depends on the experimental test configuration or on the sophistication of the model. In any case, clear definitions are generally required.

Normal Shock Wave

Within the context of the analysis, a normal shock wave may be present whenever the upstream flow is supersonic. Conditions just upstream and downstream of a normal shock are denoted with u and d subscripts, respectively. Conservation of momentum across the shock is given by

$$(p + \rho V^2)_u = (p + \rho V^2)_d$$

Multiplication by $A_u = A_d$ yields

$$F_u = F_d$$

and the impulse function does not change across a normal shock.

In certain circumstances, a change in location of a normal shock inside a duct does not alter the impulse function at the exit plane of the duct. The one nontrivial example of this is Rayleigh flow as shown on pp. 123-125 of reference 10.

More generally, however, the location of a shock wave does alter the exit plane value of the impulse function, and thereby alters the thrust. This is most readily demonstrated for a nozzle flow that contains a normal shock wave inside its divergent section. With inlet conditions fixed, the exit plane subsonic Mach number depends on the location of the shock. Consequently, the value of the exit plane impulse function also varies with the location of the shock.

As evident from figure 6, a large thrust may occur if the exit Mach number M_3 is very small compared to unity. This will occur if the back pressure of the nozzle is sufficiently high so that there is a normal shock near station 2 that occurs in either the combustor or the upstream part of the nozzle. There will be a high static temperature downstream of the shock with thermal dissociation of the normal combustion products, such as H_2O, NO_x, N_2, ... The dissociation process, of course, prevents the static temperature from escalating to an even higher value. It also represents a significant endothermic process that reduces the stagnation temperature and the thermal efficiency of the engine.

In addition to the above discussion, the presence of a normal shock, or, more realistically, a shock system, causes boundary-layer separation and high local heat transfer rates. In this circumstance, an idealized one-dimensional analysis would grossly overestimate the engine's thrust.

In view of these factors, the flow inside the engine hereafter is assumed to be free of a normal shock wave.

Influence Coefficient Method

Our discussion in this subsection does not presume inviscid flow in the combustor, except when stated. In the influence coefficient method, the quantities

$$\frac{dA}{A} \quad , \quad \frac{dT_0}{T_0} \quad , \quad 4C_f \frac{dx}{D}$$

act as forcing functions, where x is axial distance, D is the hydraulic diameter, and C_f is the skin friction coefficient. The above quantities are presumed to be known functions of either M or x. Once known, other variables are determined by equations such as equations (8.7) in reference 10. Our analysis utilizes three such equations:

$$\frac{dF}{F} = \frac{1}{1 + \gamma M^2} \frac{dA}{A} - \frac{\gamma}{2} \frac{M^2}{1 + \gamma M^2} \left(4C_f \frac{dx}{D}\right) \tag{39}$$

$$\frac{M^2 - 1}{1 + \frac{\gamma-1}{2} M^2} \frac{dM^2}{M^2} = 2 \frac{dA}{A} - \left(1 + \gamma M^2\right) \frac{dT_0}{T_0} - \gamma M^2 \left(4C_f \frac{dx}{D}\right) \tag{40}$$

$$\frac{M^2 - 1}{\gamma M^2} \frac{dp}{p} = - \frac{dA}{A} + \left(1 + \frac{\gamma-1}{2} M^2\right) \frac{dT_0}{T_0} + \left(\frac{1}{2} + \frac{\gamma-1}{2} M^2\right) \left(4C_f \frac{dx}{D}\right) \tag{41}$$

Equation (39) is equation (8.12) in reference 10, while equations (40) and (41) are taken from p. 433 of this reference. Although dT_0 does not appear in equation (39), the impulse function depends on the heat addition through changes in the Mach number. The above relations stem from the one-dimensional conservation equations for a steady flow, the state equations of a perfect gas, and the definitions of the impulse function and Mach number.

If we logarithmically differentiate equation (37a) with $\dot{m} = 0$ and substitute the resulting value for dF/F into equation (39), we obtain equation (40). Thus, equation (37a) is an exact solution of equations (39) and (40). We thus write

$$\frac{F}{F_1} = \frac{M_1}{M} \frac{1 + \gamma M^2}{1 + \gamma M_1^2} \left(\frac{1 + \frac{\gamma-1}{2} M_1^2}{1 + \frac{\gamma-1}{2} M^2} \right)^{1/2} \left(\frac{T_0}{T_{01}} \right)^{1/2} \tag{42}$$

for the flow in the combustor. If $dA = C_f = 0$, we have Rayleigh flow for which we can show that $\mathcal{T}_{1-2} = 0$. When $C_f \neq 0$ and $dA = 0$, it is the skin friction that provides the thrust even though C_f does not appear in equation (42). In this circumstance, we can show that $\mathcal{T}_{1-2} < 0$, irrespective of the value of M_1.

We can now write for a combustor with skin friction and a variable cross-sectional area

$$\frac{F_2}{F_1} = \frac{M_1}{M_2} \frac{1 + \gamma M_2^2}{1 + \gamma M_1^2} \left(\frac{1 + \frac{\gamma-1}{2} M_1^2}{1 + \frac{\gamma-1}{2} M_2^2} \right)^{1/2} \left(\frac{T_{02}}{T_{01}} \right)^{1/2} \tag{43}$$

This relation shows the importance of a large Q, or T_{02}/T_{01}, value for increasing F_2 relative to F_1.

From equation (39), we observe that friction always produces a negative dF. The effect of heat addition is not so simple, especially at supersonic speeds. While heat addition may increase F because of the stagnation temperature ratio in equation (42), it also alters the Mach number. At supersonic speeds, the Mach number decreases due to heat addition, thereby tending to decrease F. These opposite trends suggest a solution that would

maximize the thrust of the combustor. We address this question in the next section.

ANALYSIS

Thrust

Within the context of the analysis, the two thrusts of interest are written as

$$\mathcal{T}_{1-2} = \left(1 + \gamma M_1^2\right) \left(\frac{1 + \frac{\gamma-1}{2} M_\infty^2}{1 + \frac{\gamma-1}{2} M_1^2}\right)^{\gamma/(\gamma-1)} \left(\frac{F_2}{F_1} - 1\right) \tag{44a}$$

$$\mathcal{T}_{1-3} = \left(1 + \gamma M_1^2\right) \left(\frac{1 + \frac{\gamma-1}{2} M_\infty^2}{1 + \frac{\gamma-1}{2} M_1^2}\right)^{\gamma/(\gamma-1)} \left(\frac{F_2}{F_1} \frac{F_3}{F_2} - 1\right) \tag{44b}$$

where F_2/F_1 is given by Eq. (43) and F_3/F_2 by equation (38). We presume all Mach numbers are sonic or supersonic, $M_\infty \geq M_1$, $M_3 \geq M_2$, and M_2 may be greater or less than M_1.

Several general conclusions can be drawn from equations (44). First, if

$$\frac{F_2}{F_1} > 1 \quad \text{and} \quad M_3 > M_2 \tag{45}$$

we have

$$\mathcal{T}_{1-3} > \mathcal{T}_{1-2} > 0$$

It is possible for F_2/F_1 to be less than unity, in which case $\mathcal{T}_{1-2}$ is

negative. For example, this occurs when

$$Q = 0 \quad , \quad 1 \leqslant M_2 < M_1$$

An important conclusion is that $\mathcal{T}_{1-3}$ is independent of M_2. (This result does not assume an inviscid combustor.) A sonic value for M_2 means that a relatively large fraction of the thrust is produced by the nozzle. Alternatively, if $M_2 = M_3$, there is no nozzle and all of the thrust comes from the combustor.

In our analysis, various Mach numbers are prescribed rather than area ratios. As we have just shown, the overall thrust is independent of M_2 and therefore is also independent of A_2/A_1. Consequently, there is no point to maximizing the combustor thrust $\mathcal{T}_{1-2}$, since the overall thrust remains fixed.

With prescribed area ratios instead of Mach numbers, we see that the combustor thrust has a maximum value when $A_2/A_1 > 1$ and the heat addition is just sufficient to result in $M_2 = 1$. In this circumstance, the pressure p_2 at the exit of the combustor has its maximum value. (There is a structural limit on the magnitude of the combustor pressure. Because of the high aspect ratio of a roughly rectangular combustor cross section and its severe thermal environment, this pressure limit is rather low.) In any case, it is the overall thrust that should be maximized, not that of the combustor. Shortly, we derive a condition for maximizing $\mathcal{T}_{1-3}$ when the Mach numbers are prescribed.

The independent parameters in this influence coefficient model are γ, M_∞, M_1, M_2, M_3, and Q. Once these are specified, with the exception of M_2, then $\mathcal{T}_{1-3}$ is determined. Since the combustor is located inside the vehicle, it is advisable to keep A_2/A_1 from becoming unduly large. As will be shown, this is achieved by setting $M_2 = 1$. (We also discuss cases when $M_2 > 1$ and A_2/A_1 is

not unduly large.)

It is useful to write equation (44b) as

$$\mathcal{T}_{1-3} = \left(1 + \gamma M_1^2\right)\left(\frac{1 + \frac{\gamma-1}{2} M_\infty^2}{1 + \frac{\gamma-1}{2} M_1^2}\right)^{\gamma/(\gamma-1)}$$

$$\times \left[\frac{M_1}{M_3} \frac{1 + \gamma M_3^2}{1 + \gamma M_1^2} \left(\frac{1 + \frac{\gamma-1}{2} M_1^2}{1 + \frac{\gamma-1}{2} M_3^2}\right)^{1/2} \left(\frac{T_{02}}{T_{01}}\right)^{1/2} - 1\right] \tag{46}$$

We suppose M_∞, M_3, and T_{02}/T_{01} are kept fixed, and examine the dependence of $\mathcal{T}_{1-3}$ on M_1. We, therefore, write this relation as

$$\mathcal{T}_{1-3} = \frac{BM_1}{\left(1 + \frac{\gamma-1}{2} M_1^2\right)^{(\gamma+1)/[2(\gamma-1)]}} - \frac{C\left(1 + \gamma M_1^2\right)}{\left(1 + \frac{\gamma-1}{2} M_1^2\right)^{\gamma/(\gamma-1)}} \tag{47}$$

where the fixed parameters B and C are

$$B = \frac{\left(1 + \frac{\gamma-1}{2} M_\infty^2\right)^{\gamma/(\gamma-1)} \left(1 + \gamma M_3^2\right)}{M_3\left(1 + \frac{\gamma-1}{2} M_3^2\right)^{1/2}} \left(\frac{T_{02}}{T_{01}}\right)^{1/2}$$

$$C = \left(1 + \frac{\gamma-1}{2} M_\infty^2\right)^{\gamma/(\gamma-1)}$$

An extremum value of $\mathcal{T}_{1-3}$ is found by differentiating equation (47) with respect to M_1, with the result

$$\frac{\partial \mathcal{T}_{1-3}}{\partial M_1} = \frac{\left(M_1^2 - 1\right)}{\left(1 + \frac{\gamma-1}{2} M_1^2\right)^{(3\gamma-1)/[2(\gamma-1)]}} \left[\frac{\gamma C M_1}{\left(1 + \frac{\gamma-1}{2} M_1^2\right)^{1/2}} - B\right]$$

By setting the right side equal to zero, we obtain

$$M_1 = 1 \tag{48}$$

which yields a maximum value, $\mathcal{T}_{1-3,mx}$, given by

$$\mathcal{T}_{1-3,mx} = \left(\frac{2}{\gamma+1}\right)^{(\gamma+1)/[2(\gamma-1)]} \left(1 + \frac{\gamma-1}{2} M_\infty^2\right)^{\gamma/(\gamma-1)}$$

$$\times \left\{\frac{\left(1 + \gamma M_3^2\right)}{M_3\left(1 + \frac{\gamma-1}{2} M_3^2\right)^{1/2}} \left(\frac{T_{02}}{T_{01}}\right)^{1/2} - [2(\gamma+1)]^{1/2}\right\} \tag{49}$$

The other root

$$\left(1 + \frac{\gamma-1}{2} M_1^2\right)^{1/2} B = \gamma C M_1$$

yields a negative value for $\mathcal{T}_{1-3}$, and therefore is of no interest.

From equation (46), we observe that the largest permissible values for M_∞, M_3, and T_{02}/T_{01} yields a maximum value for $\mathcal{T}_{1-3}$. The result for M_3 is evident from equation (42) and figure 6. These parameters, however, are constrained by a number of conditions, such as a maximum combustor static temperature.

Area and Pressure Ratios

We obtain the pressure and area variation under the assumption of inviscid flow. For the combustor, this is accomplished by integrating

equations (40) and (41) with $C_f = 0$. The results for the nozzle integration, where we also have $dT_0 = 0$, are provided by the isentropic results, equations (24) and (25). Aside from isentropic flow, there are two other simple special cases for the combustor. In the first of these, we assume $dA = 0$. This yields the Rayleigh flow solution, which requires $Q_R \geq Q$. Neither this solution nor the isentropic one are of interest for the combustor.

The last special combustor case, $dM^2 = 0$, easily yields for the area ratio

$$\frac{A}{A_1} = \left(\frac{T_0}{T_{01}}\right)^{(1+\gamma M^2)/2} \tag{50a}$$

With the aid of equation (41), the pressure variation is

$$\frac{p}{p_1} = \left(\frac{T_0}{T_{01}}\right)^{-\gamma M^2/2} \tag{50b}$$

For $\gamma = 1.4$ and $M = 1$, the area grows slightly faster than linear with T_0/T_{01}. For moderate supersonic Mach numbers, the rate of growth can still be relatively slow when T_0/T_{01} does not rapidly increase with x.

We perform the integration of equation (40) for the combustor by arbitrarily assuming a relation between T_0 and M. The equation to be utilized is

$$\frac{T_0}{T_{01}} = \exp\left[\left(\frac{M - M_1}{M_2 - M_1}\right) \ln\left(\frac{T_{02}}{T_{01}}\right)\right] \tag{51}$$

This relation is chosen for its analytical simplicity. Other relations can be used, e.g., one for A(x) and another for $T_0(x)$. It is important to note that the combustor and overall thrust values are unaltered by any of these choices.

Equation (51) yields

$$\frac{dT_0}{T_0} = \alpha dM \tag{52}$$

where

$$\alpha = \frac{1}{M_2 - M_1} \ln \frac{T_{02}}{T_{01}} \tag{53}$$

and T_{02}/T_{01} is provided by equation (30). With equation (52) and $C_f = 0$, equation (40) becomes

$$\frac{M^2 - 1}{1 + \frac{\gamma-1}{2} M^2} \frac{dM^2}{M^2} = 2 \frac{dA}{A} - \alpha(1 + \gamma M^2) dM$$

The leftmost term integrates to

$$\int_{M_1^2}^{M^2} \frac{M^2 - 1}{1 + \frac{\gamma-1}{2} M^2} \frac{dM^2}{M^2} = \ln \left[\left(\frac{M_1}{M} \right)^2 \left(\frac{1 + \frac{\gamma-1}{2} M^2}{1 + \frac{\gamma-1}{2} M_1^2} \right)^{\frac{\gamma+1}{\gamma-1}} \right]$$

We thereby obtain

$$\frac{A}{A_1} = \frac{M_1}{M} \left(\frac{1 + \frac{\gamma-1}{2} M^2}{1 + \frac{\gamma-1}{2} M_1^2} \right)^{\frac{\gamma+1}{2(\gamma-1)}} \exp\left\{ \frac{\alpha}{2} \left[(M - M_1) + \frac{\gamma}{3} \left(M^3 - M_1^3 \right) \right] \right\} \tag{54}$$

for the variation of the combustor's cross-sectional area with Mach number. [The variation of A with axial distance requires specification of M(x) or its equivalent.]

The pressure ratio is evaluated by eliminating the dA terms in equations

(40) and (41), with the result

$$\frac{dp}{p} = -\frac{\gamma}{2}\left(M^2\frac{dT_0}{T_0} + \frac{dM^2}{1+\frac{\gamma-1}{2}M^2}\right) \tag{55}$$

With equation (52), this becomes

$$\frac{dp}{p} = -\frac{\gamma}{2}\left(\alpha M^2 dM + \frac{dM^2}{1+\frac{\gamma-1}{2}M^2}\right)$$

which integrates to

$$\frac{p}{p_1} = \left(\frac{1+\frac{\gamma-1}{2}M_1^2}{1+\frac{\gamma-1}{2}M^2}\right)^{\gamma/(\gamma-1)} \exp\left[-\frac{\alpha\gamma}{6}\left(M^3 - M_1^3\right)\right] \tag{56}$$

Observe that equations (54) and (56) reduce to isentropic relations when $\alpha = 0$. We attain A_2/A_1 and p_2/p_1 by simply setting $M = M_2$ in these equations. In this instance, equation (54) reduces to

$$\frac{A_2}{A_1} = \frac{\left(A_2/A_2^*\right)_{is}}{\left(A_1/A_1^*\right)_{is}}\left(\frac{T_{02}}{T_{01}}\right)^{1/2 + \gamma(M_1^2 + M_1M_2 + M_2^2)/6} \tag{57}$$

with the aid of equation (53). Here, the is subscript denotes an isentropic point relation. Note that equation (57) reduces to equation (50a) when $M_2 = M_1$. Actually, equations (51)–(54) and (56) are indeterminate when $M_2 = M_1$ in which case they are replaced by equations (50).

A useful result is obtained by considering M_1 and T_{02}/T_{01} as fixed, with

the additional restrictions:

$$M_1 \geq 1 \quad , \quad M_2 \geq 1 \quad , \quad \frac{T_{02}}{T_{01}} \geq 1$$

In this situation, $(A_2/A_2^*)_{is}$ and the (T_{02}/T_{01}) factor in equation (57) increase with M_2. Thus, A_2/A_1 is a minimum when $M_2 = 1$, with the value

$$\frac{A_2}{A_1} = \frac{\left(\frac{T_{02}}{T_{01}}\right)^{1/2 + \gamma(M_1^2 + M_1 + 1)/6}}{\left(\frac{A_1}{A_1^*}\right)_{is}} \tag{58}$$

While both numerator and denominator increase with M_1 in this relation, the numerator increases more rapidly than does the denominator. Hence, A_2/A_1 exceeds unity.

A Brayton cycle is obtained by replacing equation (52) with $dp = 0$. Equation (55) then integrates to

$$\int_{T_{01}}^{T_0} \frac{dT_0}{T_0} = -\int_{M_1^2}^{M^2} \frac{dM^2}{M^2\left(1 + \frac{\gamma-1}{2} M^2\right)}$$

$$\frac{T_0}{T_{01}} = \frac{M_1^2}{M^2} \frac{1 + \frac{\gamma-1}{2} M^2}{1 + \frac{\gamma-1}{2} M_1^2} \tag{59}$$

The heat addition Q can no longer be prescribed, since T_{02}/T_{01} is determined

by setting $M = M_2$. Alternatively, if Q is prescribed, then M_2 cannot be prescribed. In this circumstance, thermal choking must be avoided.

In this analysis, we prefer the greater flexibility of prescribing both M_2 and Q. Our results frequently correspond to a slightly favorable pressure gradient for the combustor, i.e., $p_1 > p_2$. In these cases, a Brayton cycle would result in a reduced value for the A_2/A_1 area ratio and frequently would result in thermal choking.

PARAMETRIC RESULTS

Nominal Cases

After several preliminary investigations, three nominal cases were chosen. These cases have $\gamma = 1.4$ and the values shown in table II. The nominal cases are designed to evaluate the effect of changing M_∞ with the pressure ratio p_3/p_∞ set equal to unity. This is accomplished by using

$$\frac{p_3}{p_\infty} = \frac{p_3}{p_2}\frac{p_2}{p_1}\frac{p_1}{p_\infty} = \left(\frac{1 + \frac{\gamma-1}{2} M_\infty^2}{1 + \frac{\gamma-1}{2} M_3^2}\right)^{\gamma/(\gamma-1)} \left(\frac{T_{02}}{T_{01}}\right)^{-\gamma M_2^2/2} = 1$$

where equation (50b) provides p_2/p_1. This relation then yields

$$M_3 = \left\{\frac{2}{\gamma-1}\left[\left(1 + \frac{\gamma-1}{2} M_\infty^2\right)\left(\frac{T_{02}}{T_{01}}\right)^{-(\gamma-1)M_2^2/2} - 1\right]\right\}^{1/2} \tag{60}$$

Table III lists results for these cases. We see that Q_R exceeds Q, except for the third case, and all cases adhere to an upper bound of 12.2 for T_{mx}/T_∞. With increasing M_∞, this upper bound can be met only by increasing M_1 and decreasing Q. Thus, at $M_\infty = 9$, T_{02}/T_{01} is only 1.166 although Q is still 1/3 of its value at $M_\infty = 5$. In case 3, combustor operation is either very

fuel or oxidizer rich.

Although M_1 increases with M_∞, A_2/A_1 decreases because of the decrease in T_{02}/T_{01}. The values shown for A_2/A_1 are rather modest and should be easily achieved with a practical combustor. The rapid increase in A_3/A_2 is expected, in view of the increase in M_3. All three combustors have a modest favorable pressure gradient, which should help reduce boundary-layer separation phenomena. The values in the p_3/p_2 column are to be read as 6.66×10^{-3}; they are as expected.

The final two columns show the combustor and overall thrusts. All values greatly exceed the earlier drag estimate of 206. The fraction of the overall thrust provided by the case 1 combustor is 52.5%. This large fraction occurs even though A_3/A_2 greatly exceeds A_2/A_1; it is a result of the higher pressure level in the combustor relative to the nozzle. The fraction falls rapidly with M_∞ because of the decrease in A_2/A_1. Hence, for case 3, the fraction is only 23.4%.

The rapid increase in both thrusts with M_∞ occurs despite the decrease in Q. The increase is due to the isentropic compression upstream of the combustor. This is evident from the multiplicative factor

$$\left(\frac{1 + \frac{\gamma-1}{2} M_\infty^2}{1 + \frac{\gamma-1}{2} M_1^2}\right)^{\gamma/(\gamma-1)} \tag{61}$$

that appears in equations (44). This compression corresponds to a significant value for the cross-sectional area ratio A_∞/A_1. For cases 1 and 3, this ratio is 25 and 194, respectively.

As is evident from table II, we have used a constant Mach number process for the combustor. This does not necessarily represent an optimum condition,

it merely seems to provide a better compromise for meeting the various constraints, such as a reasonable value for A_2/A_1 and a favorable pressure gradient, than alternative choices. This combustor process, however, does provide a thrust optimum when $M_1 = 1$.

For a later comparison, we need the thrust $\mathcal{T}_{1-3}$ and mass flow rate $\dot{m}$ scaled by the exit area of the nozzle. These parameters are given by

$$\frac{\hat{\mathcal{T}}_{1-3}}{A_3} = p_\infty \frac{A_1}{A_2}\frac{A_2}{A_3}\mathcal{T}_{1-3} \tag{62}$$

$$\frac{\dot{m}}{A_3} = \rho_\infty a_\infty M_1 \frac{A_1}{A_2}\frac{A_2}{A_3}\left(\frac{1+\frac{\gamma-1}{2}M_\infty^2}{1+\frac{\gamma-1}{2}M_1^2}\right)^{(\gamma+1)/[2(\gamma-1)]} \tag{63}$$

where the free stream speed of sound, a_∞, and ρ_∞ are provided by table I. We use the nozzle's exit area for the scaling, since it may be regarded as a measure of the vehicle's cross-sectional area. With $M_\infty = 7$ (case 2) and an altitude of 30 km, we obtain

$$\frac{\hat{\mathcal{T}}_{1-3}}{A_3} = 2.58 \times 10^4 \text{ Pa} \quad , \quad \frac{\dot{m}}{A_3} = 25.7 \text{ kg/m}^2\text{-s} \tag{64}$$

Since one atmosphere pressure at sea level is 1.015×10^5 Pa, the thrust level appears to be rather low. This value is placed in better perspective in the final section.

Influence of M_1, M_2, and M_3

Table IV shows the effect of varying M_1, M_2, and M_3. All cases use $\gamma = 1.4$ and the nominal cases appear as cases 1.0, 2.0, and 3.0. Variations about case 1.0 are listed as 1.xx, where xx = 1,2,..., and these cases have $M_\infty = 5$

and Q = 30. A similar statement holds for cases 2.xx and 3.xx. With the exception of cases 2.3 and 3.3, all the cases have a T_{mx}/T_{∞} below 12.2. The two exceptions exceed the T_{mx}/T_{∞} limit because $M_1 = 1$. Most cases have $M_1 = M_2$; the few exceptions are sufficient to illustrate the trends that occur when this condition doesn't hold.

With the exception of cases 1.2 and 1.3, all cases have modest values for A_2/A_1. The two exceptions demonstrate that A_2/A_1 is sensitive to M_2 when M_{∞} is relatively small. While there is a wide variation in the A_3/A_2 values, these values are nevertheless expected.

With one exception, case 1.2, all p_2/p_1 values range from 0.187 to 0.9 and a favorable pressure gradient is present in the combustor. As with A_3/A_2, p_3/p_2 has its expected values. Only the nominal cases have $p_3/p_{\infty} = 1$. A number of cases have a p_3/p_{∞} value that is below unity. Only in case 1.2, however, is the value so low that boundary-layer separation inside the nozzle would be anticipated.

The last two columns show that the thrust is not overly sensitive to small changes in M_1 when M_{∞} is small. When $M_{\infty} = 9$, however, there is considerable sensitivity. As shown by cases 1.3, 1.4, 2.5, and 2.6, this sensitivity is associated with M_1 not M_2. As previously noted, an M_1 value of unity yields a maximum value for $\mathcal{T}_{1-3}$, while a change in M_2 alters A_2/A_1, A_3/A_2, and the fraction of the thrust produced by the combustor but not the overall thrust.

Examination of cases 1.5, 1.6, 2.7, 2.8, 3.5, and 3.6 show that modest changes in M_3, as expected, have little effect on the thrust. It is worth mentioning that a modest decrease in M_3 from its nominal value produces a significant decrease in A_3/A_2. Thus, a considerable truncation of the nozzle appears to be warranted.

The M_1 and M_2 values in table IV are relatively small and don't differ appreciably. It is of interest, therefore, to consider a larger M_1 value and a wider range of M_2 values. This is done in table V, where we fix

$$\gamma = 1.4 \quad , \quad M_\infty = 9 \quad , \quad M_1 = 4 \quad , \quad M_3 = 8$$

The first three cases have Q = 10, which is the nominal value for this M_∞ value, while the last three cases have Q = 20. Within each Q group, T_{mx}/T_∞, A_3/A_2, and p_2/p_1 fall rapidly with M_2. On the other hand, A_2/A_1, p_3/p_2, and $\mathcal{T}_{1-2}$ increase rapidly with M_2. Observe that $\mathcal{T}_{1-3}$ is a constant within each group. Cases 3.7 and 3.10 have an adverse pressure gradient in the combustor even though A_2/A_1 exceeds unity. As noted, $\mathcal{T}_{1-2}$ increases rapidly with M_2 to the point where most of the thrust is generated by the combustor. In this circumstance; however, the large A_2/A_1 value may not be practical. It is important to note that the overall thrust level in this table is an order of magnitude less than that in table IV. This is a consequence of the larger M_1 value.

Influence of Q and γ

The effect of the final two parameters is shown in table IV. Except for Q and γ, all 1.xx cases have the prescribed values of the 1.0 nominal case. Examination of the T_{mx}/T_∞ column shows a considerable Q effect when M_∞ is small and a much smaller effect when M_∞ is large. The reason for this is that most of the temperature increase, when M_∞ is large, is due to the upstream isentropic compression.

The changes in $\mathcal{T}_{1-3}$ with Q are as expected. One interesting observation is the substantial thrust that occurs when Q = 0. In this case, the flow is entirely isentropic as noted earlier. Undoubtedly, a more realistic model that incorporates shock waves, skin friction, etc. would alter this finding.

Our final observation is the sensitivity to even a modest decrease in γ, especially when M_∞ is large. The increase in the thrust is entirely due to the compression upstream of the combustor as represented by the item (61) factor in equations (44). This result indicates the importance of evaluating real gas effects in the forebody and scramjet inlet regions. These effects not only include compositional changes but also vibrational excitation of air, which is significant at relatively low temperatures.

SUMMARY AND DISCUSSION

We first compare the thrust and mass flow rate values of the preceding section with that of a conventional rocket engine. For a meaningful comparison, this is done on the basis of the nozzle's exit area. For a rocket, we use the V-2 engine, whose performance has certainly been surpassed. However, data (see reference 15) for this engine is readily available, and results in

$$\frac{\hat{\mathcal{I}}}{A_3} = 5.46 \times 10^5 \text{ Pa} \quad , \quad \frac{\dot{m}}{A_3} = 274 \text{ kg/m}^2\text{-s}$$

where A_3 represents the exit nozzle area of the V-2 engine. These values are contrasted with the scramjet values in equations (64). We observe that the V-2 thrust and mass flow rate are 21 and 11 times that of the scramjet, respectively. Of course, the V-2 engine must overcome gravity for the missile, as well as a small missile drag. On the other hand, the scramjet must simply overcome drag and for this it suffices. Nevertheless, it is useful to note that the scramjet is a low power density engine, as measured by $\hat{\mathcal{I}}_{1\text{-}3}/A_3$.

Another commonly used scramjet performance parameter is the specific impulse, more properly referred to, as it sometimes is, as specific thrust. It is defined as

$$I_{sp} = \frac{\hat{\mathcal{F}}}{\dot{m}_f}$$

where $\dot{m}_f$ is the mass flow rate of the fuel. This later parameter has not appeared in the analysis because we have not evaluated $\dot{m}_f$.

The first three sections of this report are primarily tutorial. They establish the necessary background for a simple quasi-one-dimensional model for estimating scramjet performance, which is the subject of the preceding two sections. Among the various assumptions that are utilized, two standout as limiting the scope of the model. These are the assumptions of isentropic flow upstream of the combustor and of a calorically perfect, non-reacting gas. These assumptions tend to limit the validity of the model to relatively low hypersonic flight Mach numbers.

Within the constraints of the model, a number of conclusions can be drawn. These may be summarized as follows:

1. The overall thrust is a maximum when M_∞, M_3, and Q are maximum and when $M_1 = 1$. Of these conditions, a large M_∞ value and $M_1 = 1$ are the most important. When M_3 is already large compared to unity, any further increase in M_3 provides only a minimal thrust increase. While Q is more important than M_3, its effect is less important than M_1 or M_∞. As M_∞ is increased, starting from a value of about 5, M_1 must be increased above unity if the upper limit on T_{mx}/T_∞ is to be maintained. In this circumstance, a constant Mach number combustion process is found to be satisfactory, although the total thrust falls rapidly with increasing M_1.

In view of the thrust's modest dependence on Q, we believe real gas phenomena, such as vibrational excitation and molecular dissociation, needs further study. It also may be advisable to consider T_{mx}/T_∞ values greater

than 12.2, especially at large values of M_∞.

2. The fraction of the thrust associated with the combustor is substantial, often exceeding 50% of the total thrust. This fraction depends on the value of M_2. A value of $M_2 = 1$ provides a minimum value for the combustor area ratio A_2/A_1 and a maximum for the fraction of thrust produced by the nozzle.

With M_1 and M_3 prescribed, it is important to note that the total thrust is independent of M_2, even when the combustor flow is viscous. For an inviscid combustor, the thrust is independent of the heat addition distribution inside the combustor.

3. In view of items 1 and 2, the M = 1 relation for the combustor represents an optimum thrust condition. In this circumstance, the thrust is a maximum and the combustor area ratio is a minimum. This condition represents an area ruling relation for the combustor. In other words, when the variation in stagnation enthalpy is known as a function of axial distance, the combustor's cross-sectional area, A(x), can be determined. As noted, when M_∞ increases, the value of T_{mx}/T_∞ becomes a constraint that requires M_1 to exceed unity. In this circumstance, the combustor condition, dM = 0, appears to be a suitable alternative that provides a modest favorable pressure gradient for the combustor.

4. The thrust is sensitive to the value of the ratio of specific heats. This effect is due to the large compression that occurs in the forebody and scramjet inlet. This result emphasizes the importance of properly assessing real gas phenomena in the flow upstream of the combustor.

ACKNOWLEDGMENTS

It is pleasure to thank Professor M.L. Rasmussen for suggesting this study and for his critique of it. Thanks are also due Mr. Y.-Y. Bae for expertly performing the computations shown in tables II-VI and in figures 5 and 6.

REFERENCES

1. Drummond, J.P. and Weidner, E.H., "Numerical Study of a Scramjet Engine Flowfield," AIAA J. 20, pp. 1182-1187 (1982).

2. Van Wie, D.M., White, M.E., and Waltrup, P.J., "Application of Computational Design Techniques in the Development of Scramjet Engines," AIAA preprint, AIAA-87-1420, June 1987.

3. Weber, R.J. and MacKay, J.S., "An Analysis of Ramjet Engines Using Supersonic Combustion," NACA TN 4386, Lewis Flight Propulsion Laboratory, Sept. 1958.

4. Dugger, G.L., "Comparison of Hypersonic Ramjet Engines with Subsonic and Supersonic Combustion," in Combustion and Propulsion, 4th AGARD Colloq., Pergamon Press, NY, 1961, pp. 84-119.

5. Mordell, D.L. and Swithenbank, J., "Hypersonic Ramjets," in Adv. in Aeron. Sci. 4, Proc. 2nd Int. Cong. Aeron. Sci., Pergamon Press, 1962, pp. 831-848.

6. Small, W.J., Weidner, J.P., and Johnston, P.J., "Scramjet Nozzle Design and Analysis as Applied to a Highly Integrated Hypersonic Research Airplane," NASA TN D-8334, Langley Research Center, Nov. 1976.

7. Chaput, A.J., "Preliminary Sizing Methodology for Hypersonic Vehicles," AIAA preprint, AIAA-87-2954, Sept. 1987.

8. Kim, B.S., "Optimization of Waverider Configurations Generated from Non-Axisymmetric Flows Past a Nearly Circular Cone," Ph.D. Dissertation, University of Oklahoma, Norman, OK, 1983.

9. Rasmussen, M.L., "Waverider Configurations Derived from Inclined Circular and Elliptic Cones," J. of Spacecraft and Rockets, 17, pp. 537-545 (1980).

10. Emanuel, G., Gasdynamics: Theory and Applications, AIAA Education Series, NY, 1986.

11. Shapiro, A.H., Compressible Fluid Flow, Vol. I, the Ronald Press Co., NY, 1953, pp. 100-103.

12. Standard atmosphere data, NACA TN 1428.

13. Vincenti, W.G. and Kruger, C.H., Jr., Introduction to Physical Gas Dynamics, John Wiley and Sons, NY, 1956, pp. 171-175.

14. Ames Research Staff, Equations, Tables and Charts for Compressible Flow, NACA Report 1135, 1953.

15. Sutton, G.P., Rocket Propulsion Elements, 2nd edit., John Wiley and Sons, NY, 1956, p. 32.

TABLE I. Standard Atmospheric Data[12]

h, altitude		p_∞,	ρ_∞,	T_∞,	a_∞,
km	kft	Pa	kg/m^3	K	m/s
25	82.0	2.549×10^3	4.008×10^{-2}	221.5	298.4
30	98.4	1.197×10^3	1.841×10^{-2}	226.5	301.7
35	115.	5.746×10^2	8.463×10^{-3}	236.5	308.3

TABLE II. Nominal Cases with $\gamma = 1.4$ and $(p_3/p_\infty) = 1$

Case	M_∞	M_1	M_2	M_3	Q
1.0	5	1	1	4.486	30
2.0	7	1.5	1.5	6.293	20
3.0	9	2	2	8.429	10

TABLE III. Results for the Nominal Cases of Table 2

Case	Q_R	T_{02}/T_{01}	T_{mx}/T_∞	A_2/A_1	A_3/A_2	p_2/p_1	p_3/p_2	$\mathcal{F}_{1-2}$	$\mathcal{F}_{1-3}$
1.0	0	2.429	12.14	2.900	16.36	0.5373	6.66-3	374.6	713.5
2.0	3.772	1.529	11.39	2.414	55.51	0.5123	1.73-3	1107	2884
3.0	15.68	1.166	11.14	1.661	143.2	0.6503	5.70-4	1421	6084

TABLE IV. Influence of M_1, M_2, and M_3

Case	M_1	M_2	M_3	T_{mx}/T_∞	A_2/A_1	A_3/A_2	p_2/p_1	p_3/p_2	p_3/p_∞	$\mathscr{P}_{1-2}$	$\mathscr{P}_{1-3}$
1.0	1	1	4.486	12.14	2.900	16.36	0.5373	6.66-3	1	374.6	713.5
1.1	1.2	1.2	4.486	11.31	3.812	15.88	0.4089	8.53-3	0.7609	367.4	685.4
1.2	2	2	4.486	8.095	18.69	9.696	8.34-2	2.75-2	0.1552	249.2	374.0
1.3	1	1.5	4.486	10.05	49.00	13.91	0.1929	1.29-2	0.6961	425.5	713.5
1.4	1.5	1	4.486	12.14	3.542	16.36	0.7254	6.66-3	0.6961	290.7	578.8
1.5	1	1	4	12.14	2.900	10.72	0.5373	1.25-2	1.872	374.6	691.2
1.6	1	1	5	12.14	2.900	25.00	0.5373	3.58-3	0.5373	374.6	731.7
2.0	1.5	1.5	6.293	11.39	2.414	55.51	0.5123	1.73-3	1	1107	2884
2.1	1.3	1.3	6.293	12.34	2.044	61.23	0.6051	1.31-3	1.181	1190	3314
2.2	1.7	1.7	6.293	10.47	2.920	48.81	0.4235	2.33-3	0.8267	1001	2419
2.3	1	1	6.293	13.76	1.665	65.29	0.7428	8.93-4	1.450	1242	3648
2.4	2	2	6.293	9.175	4.061	38.69	0.3045	3.69-3	0.5944	826.1	1780
2.5	1.5	2	6.293	9.175	4.437	38.69	0.1876	3.69-3	0.7805	1515	2884
2.6	2	1.5	6.293	11.39	2.155	55.51	0.8523	1.73-3	0.7805	541.5	1780
2.7	1.5	1.5	6	11.39	2.414	45.21	0.5123	2.33-3	1.343	1107	2855
2.8	1.5	1.5	7	11.39	2.414	88.54	0.5123	8.87-4	0.5123	1107	2941
3.0	2	2	8.429	11.14	1.661	143.2	0.6503	5.70-4	1	1422	6084
3.1	1.8	1.8	8.429	12.17	1.530	167.9	0.7057	4.19-4	1.085	1624	7677
3.2	2.2	2.2	8.429	10.19	1.818	120.5	0.5941	7.79-4	0.9136	1226	4756
3.3	1	1	8.429	16.71	1.203	241.6	0.8980	1.38-4	1.381	2137	13549
3.4	2.5	2.5	8.429	8.914	2.115	91.63	0.5105	1.24-3	0.7850	961.8	3244
3.5	2	2	8	11.14	1.661	112.7	0.6503	8.01-4	1.406	1422	6024
3.6	2	2	9	11.14	1.661	193.9	0.6503	3.71-4	0.6503	1422	6152

TABLE V. Influence of M_2

Case	M_2	Q	T_{mx}/T_∞	A_2/A_1	A_3/A_2	p_2/p_1	p_3/p_2	p_3/p_∞	$\mathcal{T}_{1-2}$	$\mathcal{T}_{1-3}$
3.7	3	10	7.163	1.608	44.89	1.097	3.762-3	0.5736	81.00	498.5
3.8	4	10	4.776	6.038	17.74	0.1789	1.555-2	0.3866	259.8	498.5
3.9	5	10	3.343	22.44	7.604	3.220-2	5.419-2	0.2426	364.2	498.5
3.10	2	20	12.73	1.184	112.7	2.979	8.01-4	0.3318	-17.66	756.8
3.11	3	20	8.184	5.426	44.89	0.3474	3.762-3	0.1817	310.5	756.8
3.12	4	20	5.456	28.68	17.74	4.025-2	1.555-2	8.700-2	501.6	756.8

TABLE VI. Influence of Q and γ

Case	Q	γ	T_{mx}/T_∞	A_2/A_1	A_3/A_2	p_2/p_1	p_3/p_2	$\mathcal{T}_{1-2}$	$\mathcal{T}_{1-3}$
1.0	30	1.4	12.14	2.900	16.36	0.5373	6.66-3	374.6	713.5
1.7	0	1.4	5	1	16.36	1	6.66-3	0	217.5
1.8	10	1.4	7.381	1.596	16.36	0.7614	6.66-3	144.2	408.4
1.9	20	1.4	9.762	2.232	16.36	0.6260	6.66-3	266.5	570.4
1.10	30	1.35	11.19	2.862	20.55	0.5466	5.53-3	467.3	936.3
1.11	30	1.30	10.15	2.812	26.97	0.5574	4.42-3	609.7	1297
2.0	20	1.4	11.39	2.414	55.51	0.5123	1.73-3	1107	2884
2.9	10	1.4	9.419	1.627	55.51	0.6910	1.73-3	582.8	2199
2.10	30	1.4	13.36	3.361	55.51	0.3984	1.73-3	1588	3512
2.11	20	1.35	10.59	2.396	81.73	0.5183	1.22-3	1650	4600
2.12	20	1.30	9.694	2.372	131.4	0.5254	7.96-4	2702	8162
3.0	10	1.4	11.14	1.661	143.2	0.6503	5.70-4	1422	6084
3.13	0	1.4	9.556	1	143.2	1	5.70-4	0	4317
3.14	20	1.4	12.73	2.577	143.2	0.4479	5.70-4	2745	7729
3.15	10	1.35	10.45	1.657	245.0	0.6532	3.45-4	2439	11386
3.16	10	1.30	9.661	1.651	480.2	0.6568	1.83-4	4807	24844

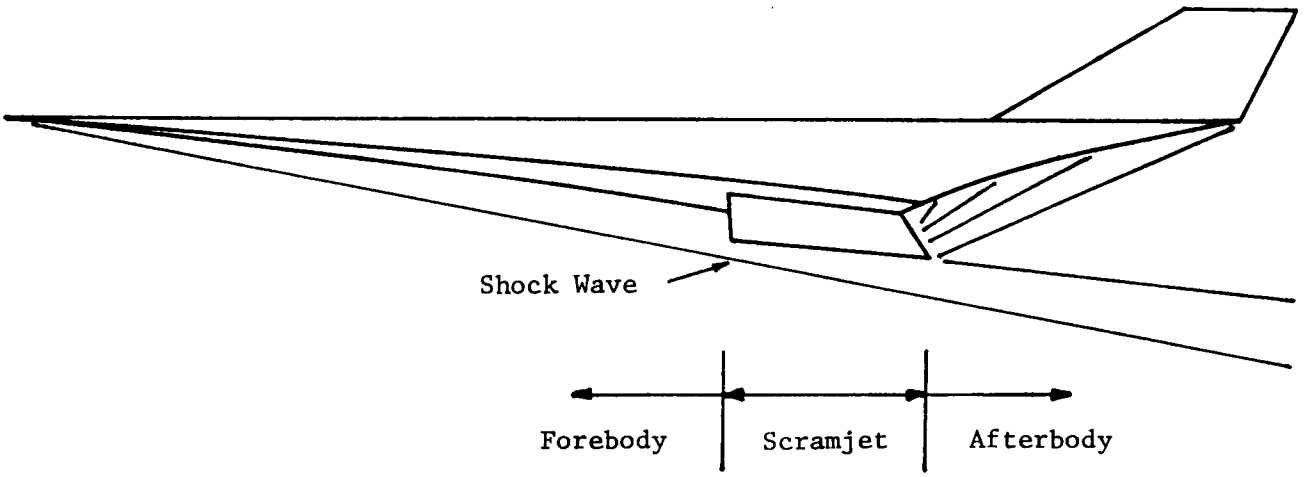

Fig. 1. Configuration for an aero-space plane.

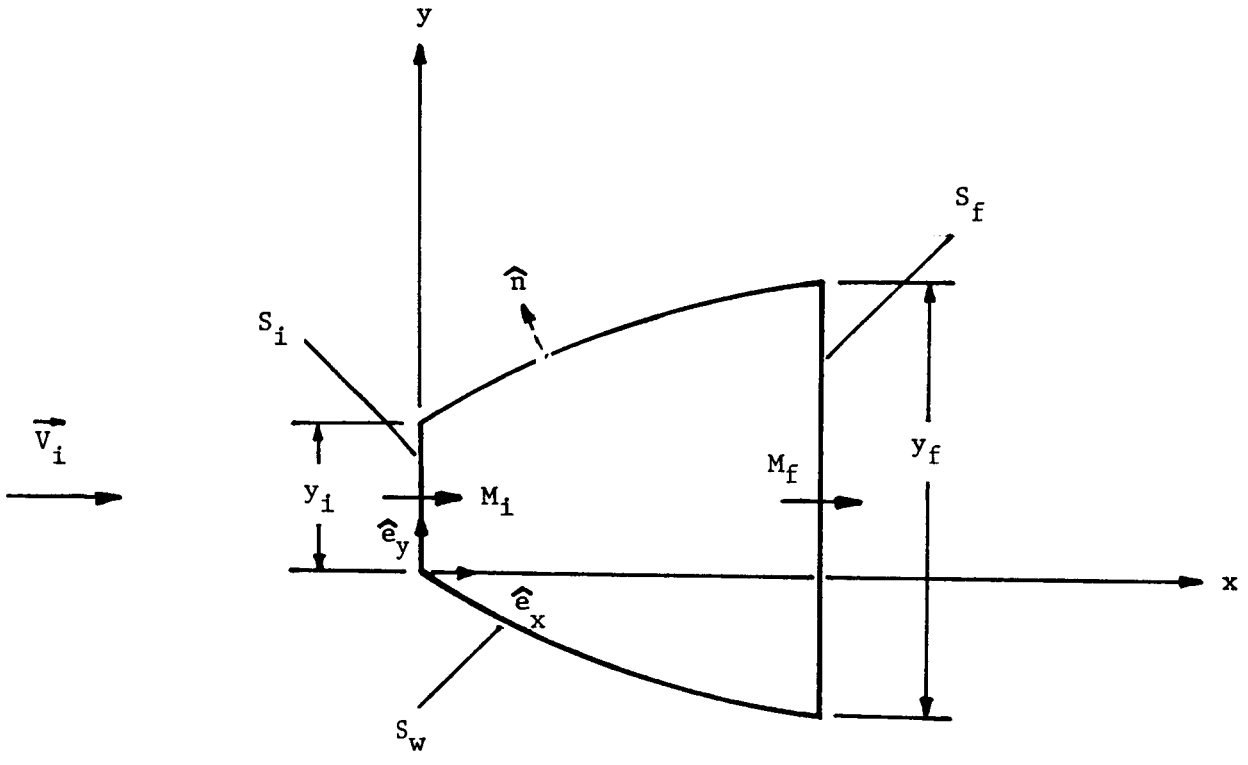

Fig. 2. Schematic of a confined nozzle.

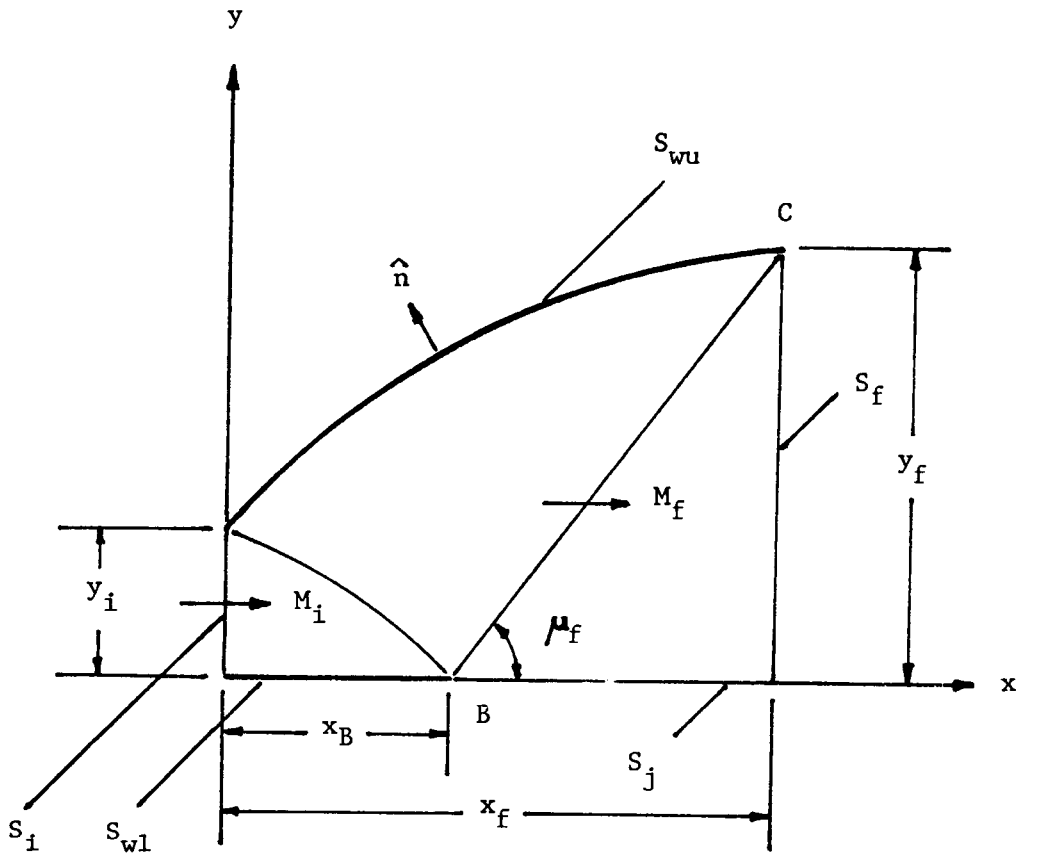

Fig. 3. Schematic of an exposed half nozzle.

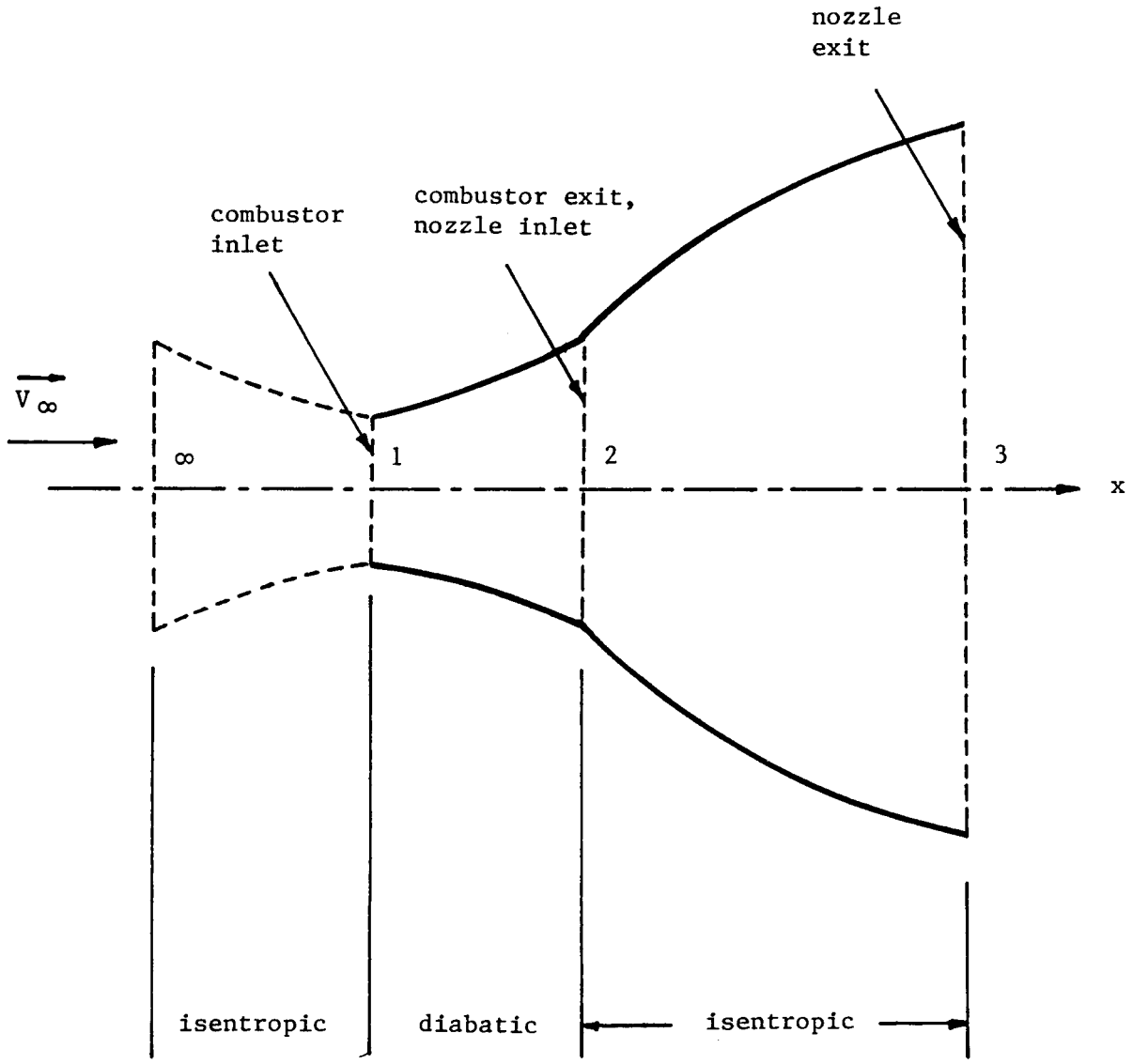

Fig. 4. Scramjet schematic.

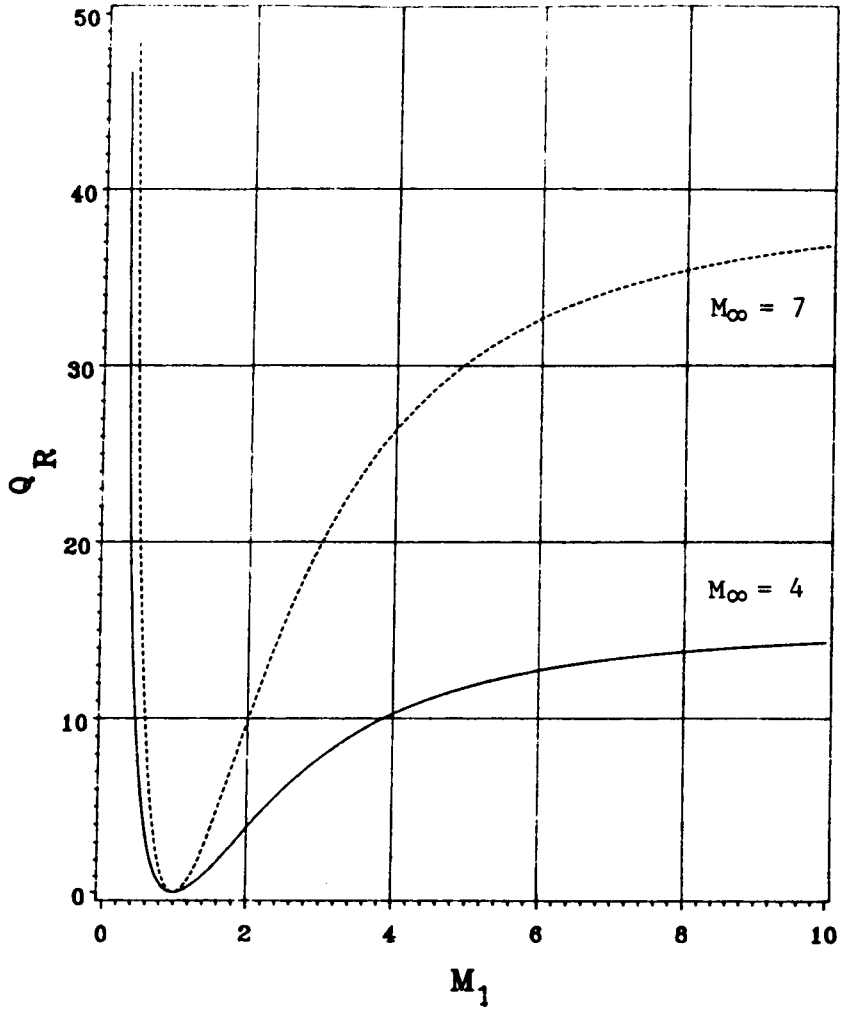

Fig. 5. Q_R vs M_1 for various M_∞ values and γ = 1.4.

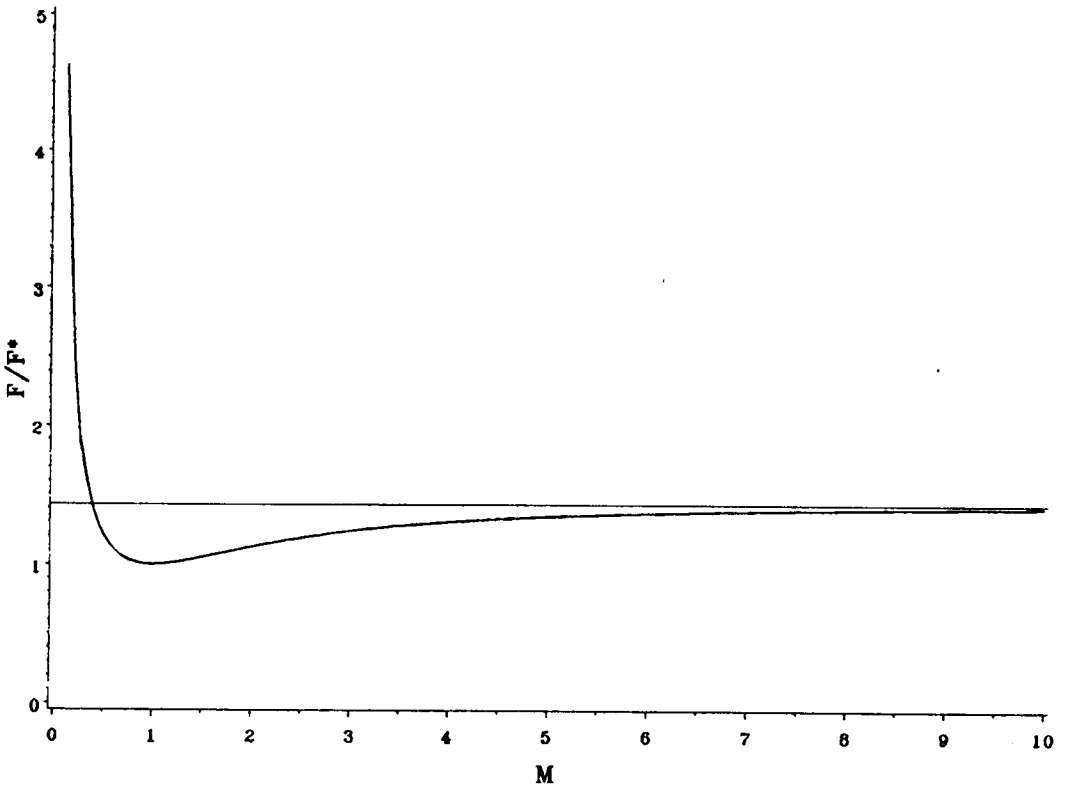

Fig. 6. F/F^* vs M for $\gamma = 1.4$.